Existence and design of trans-vacuum-speed metamaterials

Richard W. Ziolkowski* and Ching-Ying Cheng
Department of Electrical and Computer Engineering, University of Arizona, 1230 E. Speedway Boulevard, Tucson, Arizona 85721-0104, USA
(Received 23 December 2002; published 25 August 2003)

The existence of passive metamaterials, in which the speed of light is greater than its speed in vacuum, is proposed. Analysis and numerical simulations demonstrate these trans-vacuum-speed (TVS) properties. A transmission line realization of a TVS medium is established. Excellent agreement between the results of the theoretical constructs and the corresponding transmission line models are demonstrated. A practical transmission line TVS metamaterial design is proposed and validated numerically, which could be used to confirm these results experimentally.

DOI: 10.1103/PhysRevE.68.026612 PACS number(s): 41.20.Jb, 03.50.De, 84.40.Az, 81.05.Zx

I. INTRODUCTION

The issue of Einstein causality has been scrutinized extensively in recent years. The concepts of phase, group, energy, and front speeds have been analyzed and tested in a variety of different ways (for instance, Refs. [1–24]. Many of these issues have been reviewed recently by Milonni in Ref. [25] and discussed at length at the 2002 Quantum Optics Workshop at the Kavli Institute for Theoretical Physics [26].

In Ref. [27], it was shown numerically that the propagation of a pulsed plane wave through a two-time-derivative Lorentz material (2TDLM) slab allowed, in practice, the possibility of superluminal transmission of information without a violation of causality. The 2TDLM model arose from the study of artificial molecules [28–35] and absorbing boundary conditions for the finite difference time domain (FDTD) numerical solutions of Maxwell's equations [28,36–41].

A possible realization of the 2TDLM slab could be achieved through the use of metamaterials (MTMs), i.e., artificially constructed materials with electromagnetic properties not generally found in nature [42–63]. New physics issues and engineering opportunities associated with the MTMs are being explored. Metamaterial realizations, for instance, of Double Negative (DNG) media, i.e., media having both permittivity and permeability less than zero, have been designed and tested. A number of applications have been suggested, which include subwavelength imaging [44] and efficient electrically small antennas [64].

The need to revisit the propagation of electromagnetic waves in a 2TDLM medium stems from the fact that the 2TDLM model itself suggests the unorthodox position that the index of refraction at infinite angular frequency satisfies: $n(\infty)<1$. As will be discussed, this implies a violation of the principle that there is no medium in which light travels faster than its free-space value c. Such a situation has been discussed previously, in regards to light propagation in a Casimir effect configuration in the presence of zero-point fluctuations of the vacuum [65–70]. In Ref. [70], a choice of explanations for the results was posed between either the true signal speed exceeding c or the vacuum acting unstably, hence, acting as an amplifier. In contrast, it will be shown below that the 2TDLM MTM under consideration is passive and there is simply no alternative to the fact that the wave speed exceeds c in this medium. To achieve this end, the relationship between the light front speed and wave causality will be revisited to establish a common framework from which to claim that the (front) speed of light in a specifically designed 2TDLM MTM can causally exceed its value in vacuum. We will call this unusual causal medium a trans-vacuum-speed (TVS) MTM to distinguish it from superluminal propagation effects, i.e., the speed of light in such a TVS MTM is simply greater than its speed in vacuum. The propagation effects in the TVS MTM are examined analytically and numerically. It is shown that the ideal 2TDLM MTM supports front speeds greater than c. It is also shown that the behavior at infinity can be suppressed using low-pass filters and that the essence of the transmission of information propagating at speeds greater than c can be preserved. We then demonstrate that analogous to the DNG MTM results reported in Refs. [59–62], a transmission line configuration can be introduced, which yields the TVS MTM behavior. Its analytical and numerical solutions are also obtained to confirm the unorthodox TVS behavior in a physically realizable configuration. Because a commercial design tool is used for these numerical simulations and because it is a trusted algorithm validated against a large variety of experiments, we feel strongly that the results presented here are verifiable in practice. An experimental composite transmission line validation of the TVS MTM concept is proposed.

II. CAUSAL MEDIA

Causality is often associated with the constitutive relationship between the displacement (magnetic induction) field and the electric (magnetic) field [71]:

$$\mathcal{D}_x(z,t)=\varepsilon_0\mathcal{E}_x(z,t)+\int_{-\infty}^{\infty}\mathcal{G}(\tau)\mathcal{E}_x(z,t-\tau)d\tau,$$

$$\mathcal{D}_x(z,t)=\varepsilon_0\mathcal{E}_x(z,t)+\frac{1}{2\pi}\int_{-\infty}^{\infty}\chi(\omega)E_x(z,\omega)e^{+j\omega t}\,d\omega, \quad (1)$$

*FAX: (520) 621-8076;
email address: ziolkowski@ece.arizona.edu

where the response of susceptibility

$$\mathcal{G}(t)=\frac{1}{2\pi}\int_{-\infty}^{\infty}\chi(\omega)e^{+j\omega t}\,d\omega \tag{2}$$

is causal, i.e., $\mathcal{G}(t)=0$ for $t<0$. The latter will occur if susceptibility $\chi(\omega)$ is analytic in the lower half plane. For the sake of simplicity, spatially varying medium effects are ignored. If, in addition (as is required for the pulse propagation experiments discussed below), the initial condition on the electric field, $\mathcal{E}_x(0,t)=f(t)=0$ for $t<0$, is imposed, the constitutive relation becomes

$$\mathcal{D}_x(z,t)=\varepsilon_0\mathcal{E}_x(z,t)+\int_0^t\mathcal{G}(\tau)\mathcal{E}_x(z,t-\tau)d\tau. \tag{3}$$

It is generally assumed, because of causality and hence, satisfaction of the Kramers-Krönig relations, that the susceptibility must go to zero as the angular frequency goes to infinity, i.e., $\lim_{\omega\to\infty}\chi(\omega)\to 0$. However, this is not required for integral (2) to yield a causal result. In fact, if $|\chi(\omega)|$ is bounded as $|\omega|\to\infty$ and $\lim_{\omega\to\infty}\{|\chi(\omega)|/|\omega|\}=0$, then $\chi(\omega)$ has a removable singularity at infinity [72]. Then, one could rewrite Eq. (3) as

$$\mathcal{D}_x(z,t)=\varepsilon_\infty\mathcal{E}_x(z,t)+\int_0^t d\tau\,\mathcal{G}_\infty(\tau)\mathcal{E}_x(z,t-\tau),$$

$$\mathcal{D}_x(z,t)=\varepsilon_\infty\mathcal{E}_x(z,t)+\frac{1}{2\pi}\int_{-\infty}^{\infty}[\chi(\omega)-\chi_\infty]E_x(z,\omega)e^{+j\omega t}\,d\omega, \tag{4}$$

where

$$\chi_\infty=\lim_{\omega\to\infty}\chi(\omega),$$

$$\varepsilon_\infty=\varepsilon_0(1+\chi_\infty),$$

$$\mathcal{G}_\infty(t)=\frac{1}{2\pi}\int_{-\infty}^{\infty}[\chi(\omega)-\chi_\infty]e^{+j\omega t}\,d\omega. \tag{5}$$

The term $[\varepsilon(\omega)-\varepsilon_\infty]$ is now analytic for all $\mathrm{Im}\,\omega<0$ and $\mathcal{G}_\infty(t)$, like $\mathcal{G}(t)$, is causal. The Kramers-Krönig relations corresponding to this result follow immediately, as

$$\varepsilon_{real}(\omega)-\varepsilon_\infty=\frac{1}{\pi}PV\int_{-\infty}^{\infty}d\xi\frac{\varepsilon_{imag}(\omega)}{\xi-\omega},$$

$$\varepsilon_{imag}(\omega)=-\frac{1}{\pi}PV\int_{-\infty}^{\infty}d\xi\frac{\varepsilon_{real}(\omega)-\varepsilon_\infty}{\xi-\omega}. \tag{6}$$

This form is found in a variety of textbooks, e.g., Ref. [73], and affirms the footnote given in Ref. [74]. It recovers the usual form when $\varepsilon_\infty=\varepsilon_0$. Nonetheless, as just demonstrated, mathematical causality itself does not prevent the case in which $\varepsilon_\infty\neq\varepsilon_0$.

Note, however, that the requirement for having a removable singularity at infinity signifies that if the susceptibility is a rational function in ω, then it must have the form

$$\chi(\omega)=\frac{\sum_{\ell=0}^{p}\alpha_\ell\omega^\ell}{\sum_{\ell=0}^{q}\beta_\ell\omega^\ell}, \tag{7}$$

where the maximum indices must satisfy $p\leqslant q$ and the constant ratio of the leading coefficients must be finite: $\alpha_p/\beta_q<\infty$.

III. TWO-TIME DERIVATIVE LORENTZ MEDIA

The 2TDLM model has been used [27] to study superluminal transmission of information. It is revisited here to make the stronger claim that it can be used to establish that the front speed of light can exceed its vacuum value. We will base our arguments on the propagation of a one dimensional, plane wave in a matched 2TDLM medium. Let the direction of propagation be along the z axis and let the electric field be linearly polarized along the x axis.

The 2TDLM model in this one-dimensional plane wave case has the following time domain form:

$$\begin{aligned}\partial_t^2\mathcal{P}_x(z,t)+\Gamma_e\partial_t\mathcal{P}_x(z,t)+\omega_{0,e}^2\mathcal{P}_x(z,t)&=\varepsilon_0\omega_{p,e}^2\chi_{\alpha,e}\mathcal{E}_x(z,t)+\varepsilon_0\omega_{p,e}\chi_{\beta,e}\partial_t\mathcal{E}_x(z,t)\\&\quad+\varepsilon_0\chi_{\gamma,e}\partial_t^2\mathcal{E}_x(z,t).\end{aligned} \tag{8}$$

Let the Fourier transform pair of the time be $\mathcal{P}_x(z,t)$, the frequency domain be $P_x(z,\omega)$, and polarization fields be defined as

$$\mathcal{P}_x(z,t)=\frac{1}{2\pi}\int_{-\infty}^{\infty}P_x(z,\omega)e^{+j\omega t}\,d\omega,$$

$$P_x(z,\omega)=\int_{-\infty}^{\infty}\mathcal{P}_x(z,t)e^{-j\omega t}\,dt. \tag{9}$$

It is assumed that all the relevant time and frequency domain quantities here will share this transform pair representation. Consequently, since one has the following well-known frequency domain relation between the polarization field, the electric field and the electric susceptibility:

$$P_x(z,\omega)=\varepsilon_0\chi_e(\omega)E_x(z,\omega), \tag{10}$$

the 2TDLM electric susceptibility has the frequency domain form

$$\chi_e(\omega)=\frac{-\omega^2\chi_{\gamma,e}+j\omega_{p,e}\chi_{\beta,e}\omega+\omega_{p,e}^2\chi_{\alpha,e}}{-\omega^2+j\Gamma_e\omega+\omega_{0,e}^2}. \tag{11}$$

It is further assumed, without loss of generality, that the magnetic susceptibility has a similar 2TDLM form, i.e.,

$$M_y(z,\omega)=\chi_m(\omega)H_y(z,\omega), \tag{12}$$

where $\chi_m(\omega)$ is given by Eq. (11) with $e\rightarrow m$. The electric permittivity and the magnetic permeability of this 2TDLM medium then have the following frequency domain forms:

$$\varepsilon(\omega)=\varepsilon_0[1+\chi_e(\omega)],$$

$$\mu(\omega)=\mu_0[1+\chi_m(\omega)]. \tag{13}$$

To simplify the discussion further, we will consider a matched medium, i.e., one in which the permittivity and permeability satisfy $\chi_e(\omega)=\chi_m(\omega)=\chi(\omega)$, where

$$\chi(\omega)=\frac{-\omega^2\chi_\gamma+j\omega_p\chi_\beta\omega+\omega_p^2\chi_\alpha}{-\omega^2+j\Gamma\omega+\omega_0^2}, \tag{14}$$

so that the wave impedance in the 2TDLM medium matches the free-space value, i.e., so that $Z(\omega)=\sqrt{\mu(\omega)/\varepsilon(\omega)}\equiv Z_0=\sqrt{\mu_0/\varepsilon_0}$.

We note that the 2TDLM model (14) satisfies $\chi(-\omega)=\chi^*(\omega)$ to guarantee that the displacement field is real, as is the electric field. The poles of the 2TDLM model occur at $\omega_\pm=-j(\Gamma/2)\pm\sqrt{\omega_0^2-\Gamma^2/4}$ and lie strictly in the lower half of the ω plane. If $\chi(\omega)=\mathrm{Re}[\chi(\omega)]-j\,\mathrm{Im}[\chi(\omega)]$, then the real and imaginary parts of susceptibility (14) are

$$\mathrm{Re}[\chi(\omega)]=\frac{(\omega_0^2-\omega^2)(\omega_p^2\chi_\alpha-\omega^2\chi_\gamma)+\omega^2\omega_p\Gamma\chi_\beta}{(\omega_0^2-\omega^2)^2+(\Gamma\omega)^2},$$

$$\mathrm{Im}[\chi(\omega)]=\omega\left\{\frac{\omega^2[\omega_p\chi_\beta-\Gamma\chi_\gamma]+\omega_p^2\Gamma\chi_\alpha-\omega_0^2\omega_p\chi_\beta}{(\omega_0^2-\omega^2)^2+(\Gamma\omega)^2}\right\}. \tag{15}$$

Clearly, the 2TDLM medium will be passive if for all ω,

$$\omega^2[\omega_p\chi_\beta-\Gamma\chi_\gamma]+\omega_p^2\Gamma\chi_\alpha-\omega_0^2\omega_p\chi_\beta>0. \tag{16}$$

This passivity constraint can be met with a large variety of the free parameters of the 2TDLM model. We also note that in this matched 2TDLM medium, the dispersion relation obtained from Maxwell's equations has the form

$$k(\omega)=\frac{\omega}{c}n(\omega),$$

$$n(\omega)=\sqrt{\frac{\varepsilon(\omega)}{\varepsilon_0}}\sqrt{\frac{\mu(\omega)}{\mu_0}}=1+\chi(\omega). \tag{17}$$

To simplify the notations yet further, let $\omega_p\equiv\omega_0$. Then, the limiting behaviors of the 2TDLM susceptibility (14) become

$$\lim_{\omega\rightarrow 0}n(\omega)=1+\chi_\alpha,$$

$$\lim_{\omega\rightarrow\infty}n(\omega)=1+\chi_\gamma. \tag{18}$$

As will be shown below, since χ_γ can be selected to be less than zero, this 2TDLM model allows for cases in which the speed of light in the medium is greater than its value in free space.

We note that in all of the cases considered below, the 2TDLM MTM will be lossy. This property of the passive 2TDLM MTM was exploited to achieve the Maxwellian perfectly matched layer, FDTD absorbing boundary conditions (ABCs) considered in Refs. [39–41]. There, the 2TDLM MTM parameters were selected to ensure a significant decay of a wave propagating in the ABC layers. Here, the resonance region, where the strong losses and the corresponding strong dispersive effects occur, will be avoided in general by a careful selection of the spectrum of the initial pulse, as well as of the 2TDLM MTM parameters. Moreover, the presence of loss in the 2TDLM model precludes a possible need to introduce infinities to guarantee satisfaction of the generalized Kramers-Krönig relations Eqs. (6).

IV. PLANE WAVE PROPAGATION

Now consider the propagation from the plane $z=0$ in this 2TDLM medium of an initial pulse $\mathcal{E}_x(z=0,t)=f(t)$, where $f(t)=0$ for $t<0$ and $F(\omega)$ is its Fourier spectrum. From Maxwell's equations, the electric field at a point $+z$ in the matched 2TDLM medium can be represented as

$$\mathcal{E}_x(z,t)=\frac{1}{2\pi}\int_{-\infty}^{\infty}F(\omega)e^{j\omega[t-n(\omega)z/c]}\,d\omega. \tag{19}$$

Let us rewrite this electric field at (z,t) as

$$\mathcal{E}_x(z,t)=\frac{1}{2\pi}\int_{-\infty}^{\infty}F(\omega)e^{j\omega(t-n_\infty z/c)}\,d\omega + \frac{1}{2\pi}\int_{-\infty}^{\infty}F(\omega)e^{j\omega[t-n_\infty z/c]} \times\{e^{-j\omega[n(\omega)-n_\infty]z/c}-1\}d\omega. \tag{20}$$

The first term is readily evaluated as

$$\frac{1}{2\pi}\int_{-\infty}^{\infty}F(\omega)e^{j\omega(t-n_\infty z/c)}\,d\omega=f(t-n_\infty z/c). \tag{21}$$

Thus, if, in fact, the medium were designed to achieve only the index value at infinity, then to maintain causality, this representation clearly requires the following constraint: $n_\infty>0$ and hence, the constraint that the constant $\chi_\gamma>-1$ in the 2TDLM model. If the second term were negligible, then the front speed of the pulse would be $v_{\mathrm{front}}=c/n_\infty=c/(1+\chi_\gamma)$. This front speed is greater than the vacuum value for $-1<\chi_\gamma<0$. For instance, if $\chi_\gamma=-0.5$, then $v_{\mathrm{front}}=2c$. While this is a narrow range of possible values for χ_γ, the existence of a TVS MTM is clearly possible when the second term is negligible.

The second term in Eq. (20) contains all of the dispersion and loss effects. It can be written in a convenient form as

$$\frac{1}{2\pi}\int_{-\infty}^{\infty} F(\omega)e^{j\omega[t-n_\infty z/c]}\{e^{-j\omega[n(\omega)-n_\infty]z/c}-1\}d\omega=\sum_{\ell=1}^{\infty}\frac{1}{2\pi\ell!}\int_{-\infty}^{\infty} F(\omega)e^{j\omega[t-n_\infty z/c]}\{-j\omega[n(\omega)-n_\infty]z/c\}^{\ell}d\omega. \quad (22)$$

Thus, if $[n(\omega)-n_\infty]\approx 0$ over a major portion of the frequency spectrum of the input pulse $F(\omega)$, then the second term in Eq. (20) is approximately zero and the pulse propagates in the 2TDLM MTM simply, according to the relation

$$\mathcal{E}_x(z,t)\approx f(t-n_\infty z/c). \quad (23)$$

The obvious desired pulse design is to arrange the pulse spectrum to be nontrivial for frequencies above resonance ω_0 of the 2TDLM medium and trivial near and below it. If the resonance of the 2TDLM medium occurs where the pulse spectrum is large, large loss and dispersive effects will occur and the pulse will become largely distorted as it propagates.

To illustrate these behaviors explicitly, a MATLAB code was constructed to calculate Eq. (19) and the various quantities associated with the pulse propagation. We will consider one of the passive 2TDLM cases given in Ref. [27], shifted to a lower frequency. Let $\chi_\alpha=1.0$, $\chi_\beta=1.0\times10^{-5}$, $\chi_\gamma=-0.5$, $\omega_p=\omega_0=2\pi f_0$, and $\Gamma=1.0\times10^{-3}\omega_0$, where $f_0=1.0\times10^6$ Hz. Since $\chi_\infty=-0.5$, the pulse front speed $v_{front}=2.0c$. The real and imaginary parts of the index of refraction n, given by Eq. (17), in the frequency domain are shown in Fig. 1.

The input pulse is assumed to be a finite width, unit amplitude pulse of time length T, which has the bipolar form

$$f(t)=\begin{cases} 0 & \text{for } t<0 \\ -\sqrt{7.0}(7.0/6.0)^3\left(\dfrac{t-T/2}{T/2}\right)\left[1-\left(\dfrac{t-T/2}{T/2}\right)^2\right]^3 & \text{for } 0\leq t\leq T \\ 0 & \text{for } t>T. \end{cases} \quad (24)$$

The value of this pulse and at least its first two derivatives are all zero at $t=0$. This input pulse and the magnitude of its Fourier spectrum when $T=10.0$ ns are shown in Fig. 2. Note that the spectrum of this pulse is centered at 100 MHz and has no dc component.

Consider now the propagation of this pulse in the specified 2TDLM MTM when $T=0.5$ μs. The magnitude of the pulse spectrum normalized to its maximum value and the un-normalized magnitude of the index of refraction of the 2TDLM MTM are shown together in Fig. 3. A considerable overlap of these spectra is observed. The initial pulse and the pulse measured at $z=60.0$ m are shown in Fig. 4. The expected pulse distortion from the medium losses and dispersion are evident. The extended observation distance was selected to extenuate these issues. In contrast, consider the propagation of the input pulse in the specified 2TDLM MTM when $T=10.0$ ns. The magnitude of the pulse spectrum normalized to its maximum value and the un-normalized magnitude of the index of refraction of the 2TDLM MTM are shown together in Fig. 5. The initial pulse and the pulse measured at $z=6.0$ m are plotted in Fig. 6. Because of the careful crafting of the pulse spectrum to avoid any overlap with the resonance region, i.e., to avoid any significant loss or dispersion, almost no distortion is seen in the propagated pulse.

Now consider the $T=10.0$ ns pulse propagating in free space and in a normal double positive (DPS) matched medium with $\varepsilon_r=2.0$ and $\mu_r=2.0$. The front speeds will be, respectively, $v_{front}=c$ and $v_{front}=c/2$. The measured pulses at $z=6.0$ m for the TVS MTM, free-space, and DPS medium cases are shown in Fig. 7. Clearly, the entire signal propagates faster than in free space in the TVS case. Moreover, by considering the pulse propagation within the same medium everywhere, there are no pulse reshaping effects to confuse the issues involved, particularly such as those that occurred in Ref. [27] when the pulse entered the 2TDLM slab from free space and left it.

V. PROPAGATION IN NONPERFECT TVS MEDIUM

As pointed out in Ref. [27], one would not expect to be able to maintain the perfect 2TDLM properties at high frequencies in any practical realization. Consequently, one has to ask: ''Will the absence of the infinite frequency properties ruin the TVS MTM propagation results?''

To force the permittivity and permeability, and hence the index of refraction, to have free-space behaviors at high frequencies, we introduce a low-pass filter into the 2TDLM response. In particular, if the low-pass filter is represented by

$$A(\omega)=\frac{1}{1+(\omega/\omega_c)^2}, \quad (25)$$

where $\omega_c=2\pi f_c$ defines the half amplitude point in its spectrum, we then create the modified loss-pass 2TDLM MTM by setting

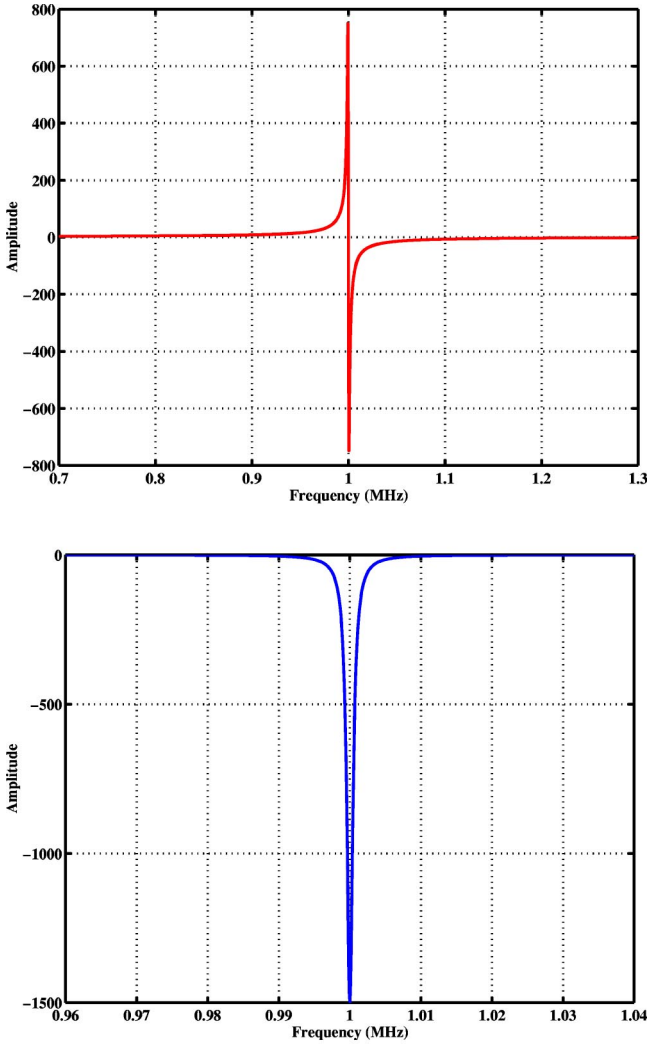

FIG. 1. (Color online) The 2TDLM MTM under consideration has an index of refraction whose resonance occurs at 1.0 MHz. (a) Real part of the index of refraction. (b) Imaginary part of the index of refraction.

$$n_{LP}(\omega) = 1.0 + A(\omega)\chi(\omega). \tag{26}$$

The resulting propagation integral becomes simply

$$\mathcal{E}_x(z,t) = \frac{1}{2\pi}\int_{-\infty}^{\infty} F(\omega) e^{j\omega[t - n_{LP}(\omega)z/c]}\, d\omega. \tag{27}$$

Its behavior is evaluated numerically, as in the previous ideal case.

In particular, consider the results obtained by setting $f_c = 10$ GHz. An overlay of the magnitudes of the input pulse spectrum normalized to its maximum value and the unnormalized magnitude of the index of refraction of the low-pass 2TDLM MTM, $n_{LP}(\omega)$, is given in Fig. 8. Note that because the resonance region is located well below the filter cutoff value f_c, losses are still present in the MTM. From Fig. 8 one observes that the index of refraction is approximately constant over the bandwidth of the input pulse, as desired. If $f_P = \omega_P/2\pi$ is the frequency of the peak of the

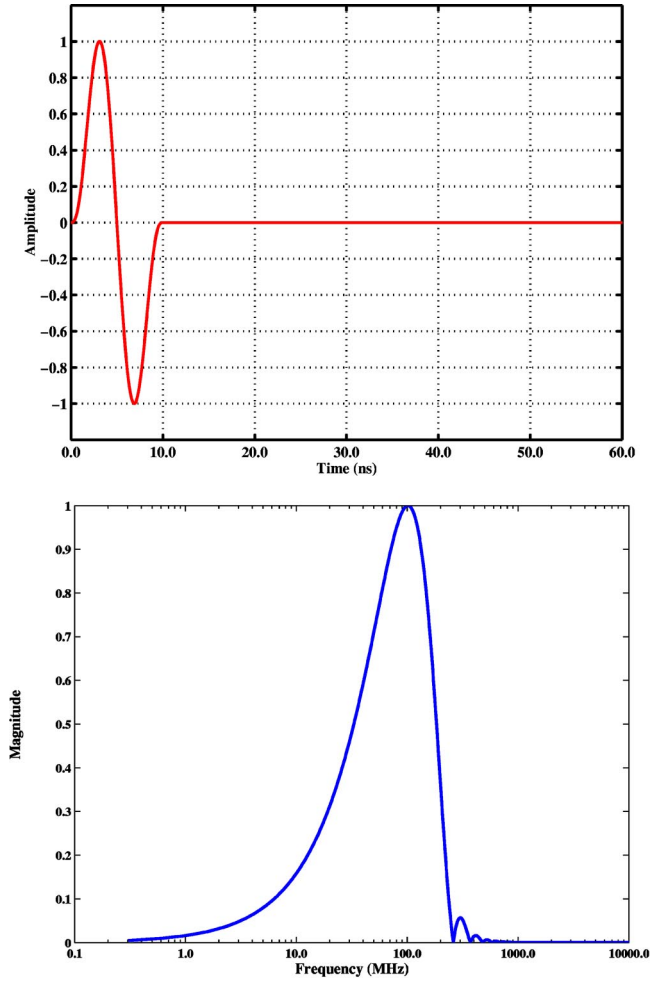

FIG. 2. (Color online) The input signal is a 10.0 ns bipolar pulse. The magnitude of its frequency spectrum, normalized to its maximum value (4.2103×10^{-9}), is centered at 100.0 MHz. (a) Input pulse. (b) Normalized input pulse spectrum.

magnitude of the spectrum, this index value is $n_{LP}(\omega_P)$. Following the arguments leading from Eqs. (19)–(23), one then finds from Eq. (27) that the pulse propagated in the modified loss-pass 2TDLM MTM should have the form

$$\mathcal{E}_x(z,t) \approx f(t - n_{LP}(\omega_P)z/c). \tag{28}$$

Since by design $f_P = 100$ MHz and $n_{LP}(\omega_P) = 0.5$, the input pulse should propagate with little distortion at the speed $c/n_{LP}(\omega_P) = 2.0c$.

The pulse predicted at the observation point $z = 6.0$ m, by calculating Eq. (27) numerically, is compared to the input pulse and the free-space propagated pulse in Fig. 9. Clearly, the modified medium has maintained the TVS properties; and Eq. (28) is a very good approximation of the propagated pulse. We reemphasize that the reason that the results are essentially identical to the ideal case is that the angular frequency behavior of the 2TDLM index of refraction away from the resonance is basically constant. By designing the pulse and its spectrum to lie in the region below the low-pass

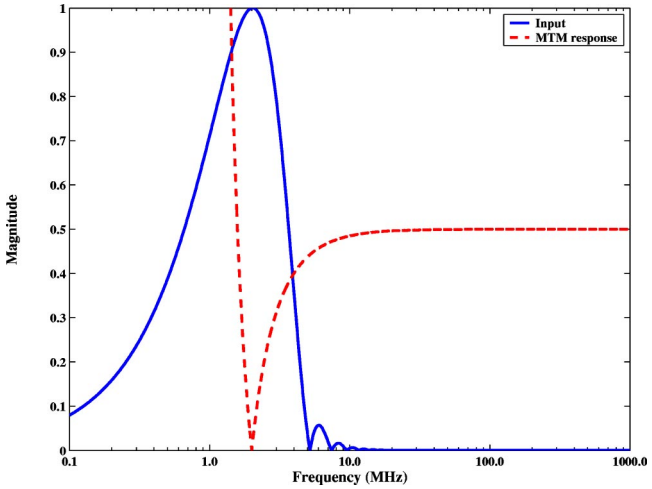

FIG. 3. (Color online) The magnitude of the spectrum of the 500.0 μs input pulse normalized to its peak value (2.1051×10^{-7}) at 2.0 MHz and the magnitude of the unnormalized spectrum of the 2TDLM MTM show a significant overlap near the resonance region.

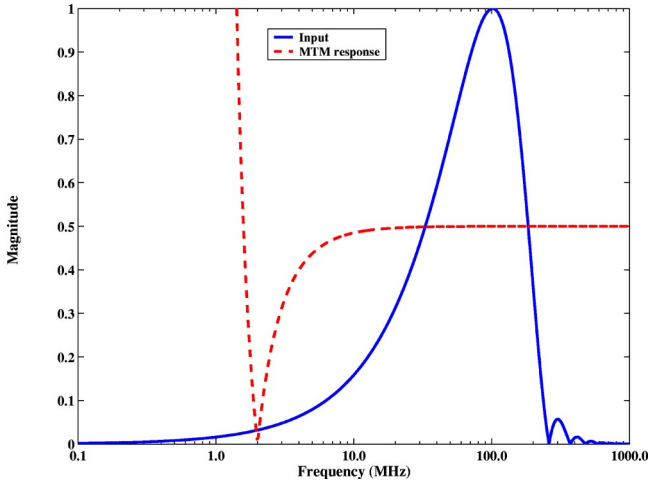

FIG. 5. (Color online) The magnitude of the spectrum of the 10.0 ns input pulse and of the magnitude of the unnormalized spectrum of the unfiltered 2TDLM MTM index of refraction show a very minor overlap of the resonance region. Most of the pulse spectrum occurs in the frequency region where $n\approx1+\chi_\gamma=0.5$.

filter's cutoff frequency f_c, yet well above the resonance frequency f_0, one is able to achieve a nearly distortion-free TVS pulse propagation.

Given the fact that the low-pass 2TDLM MTM still exhibited the TVS properties, an experimental realization was designed.

VI. ANALYTICAL TRANSMISSION LINE MODEL OF THE TVS MTM

To design a practical realization of the TVS 2TDLM MTM, it was decided to mimic the transmission line realization of a DNG metamaterial introduced by Eleftheriades [59–62]. An *ABCD* matrix approach to modeling the behavior of the two-port network that represents a transmission line configuration is widely used in microwave engineering applications. Once elementary two-port *ABCD* matrices for the various transmission line elements in a more complicated two-port network are constructed, the entire network can be easily modeled by simply cascading the connections, i.e., by simply multiplying the individual *ABCD* matrices together.

A section of an ideal lossless transmission line can be represented as [75]

$$\begin{pmatrix} A & B \\ C & D \end{pmatrix} = \begin{pmatrix} \cos(\beta\ell) & jZ_0\sin(\beta\ell) \\ jY_0\sin(\beta\ell) & \cos(\beta\ell) \end{pmatrix}, \tag{29}$$

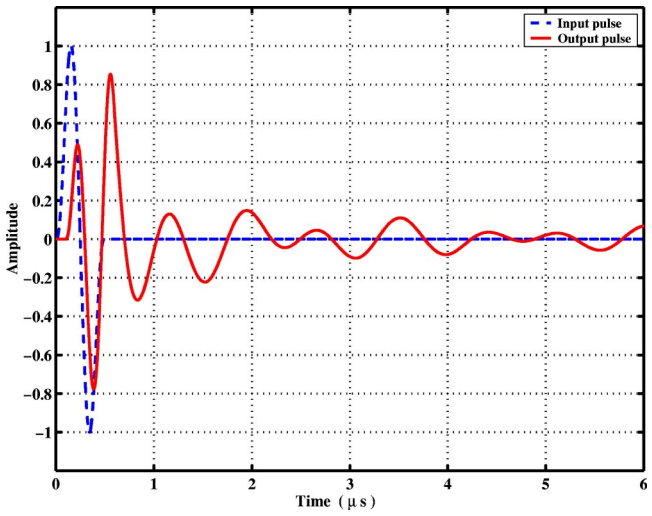

FIG. 4. (Color online) The 0.5 μs input pulse ($z=0$ m) and the pulse received at $z=60$ m after propagation through the 2TDLM MTM are compared. Significant distortion of the input pulse is present in the propagated result due to the overlap of the spectra shown in Fig. 3.

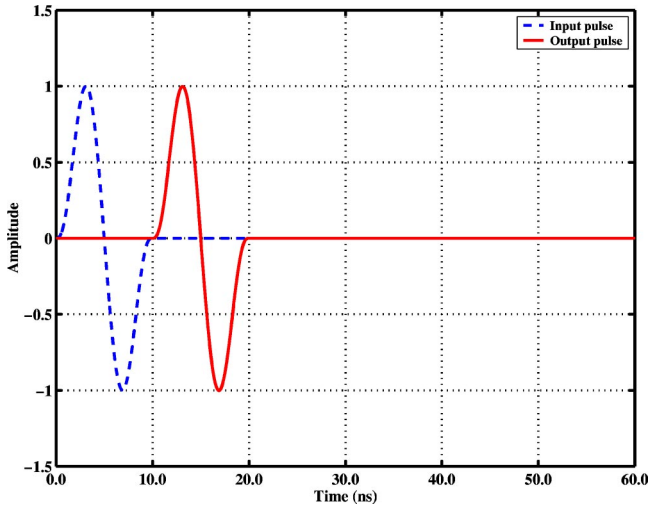

FIG. 6. (Color online) The 10.0 ns input pulse ($z=0$ m) and the pulse received at $z=6$ m after propagation through the 2TDLM MTM are compared. No apparent distortion of the input pulse is present in the propagated result. This is due to the minor overlap of the spectra shown in Fig. 5.

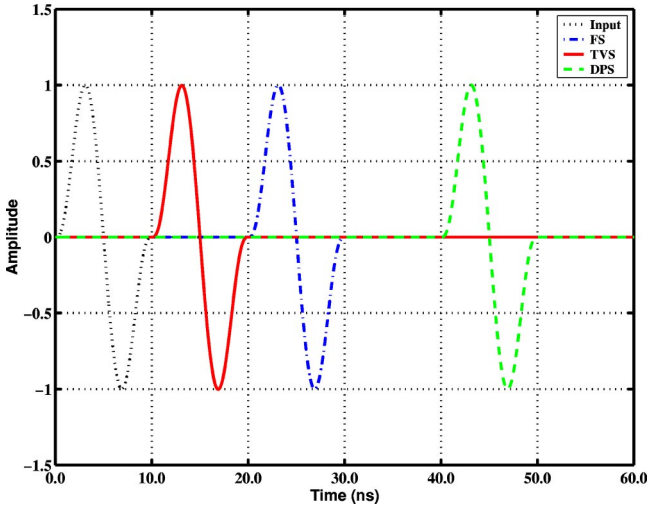

FIG. 7. (Color online) The input pulse and the pulses resulting from propagation in free space with $v_{front}=c$, in the TVS 2TDLM MTM with $v_{front}=2c$, and in a homogenous DPS medium with $\epsilon_r=2.0$ and $\mu_r=2.0$ so that $v_{front}=c/2$, are compared. The 2TDLM MTM pulse propagation clearly exhibits the predicted, unorthodox TVS behavior.

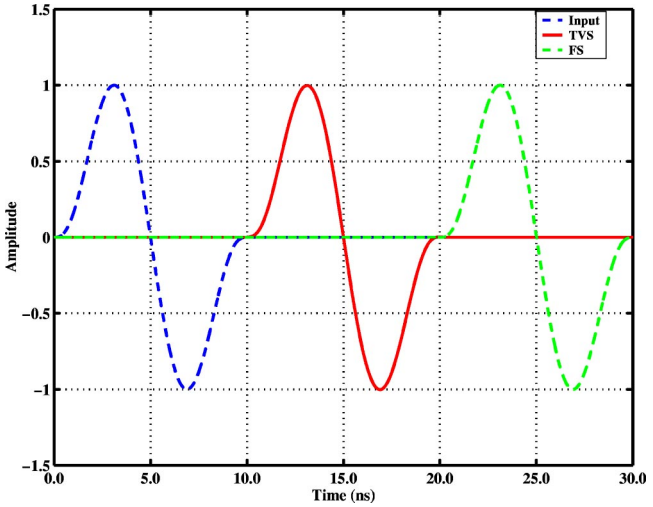

FIG. 9. (Color online) The 10.0 ns input pulse ($z=0$ m), the pulse received at $z=6$ m after propagation through the low-pass filtered 2TDLM MTM, and the pulse received at $z=6$ m after propagation through free space are compared. No apparent distortion of the input pulse is present in the 2TDLM MTM propagated result and the TVS effect is still clearly present.

where the propagation constant $\beta=2\pi/\lambda$, the length of the transmission is ℓ, and the characteristic impedance and admittance of the transmission line are Z_0 and Y_0, respectively. This expression is valid for any length of the transmission line.

If, however, the length of the lossless transmission line is small, i.e., if $\ell/\lambda \ll 1$, then the $ABCD$ parameters in Eq. (29) can be approximated as

$$\begin{pmatrix} A & B \\ C & D \end{pmatrix} = \begin{pmatrix} 1 & jZ_0\beta\ell \\ jY_0\beta\ell & 1 \end{pmatrix}. \tag{30}$$

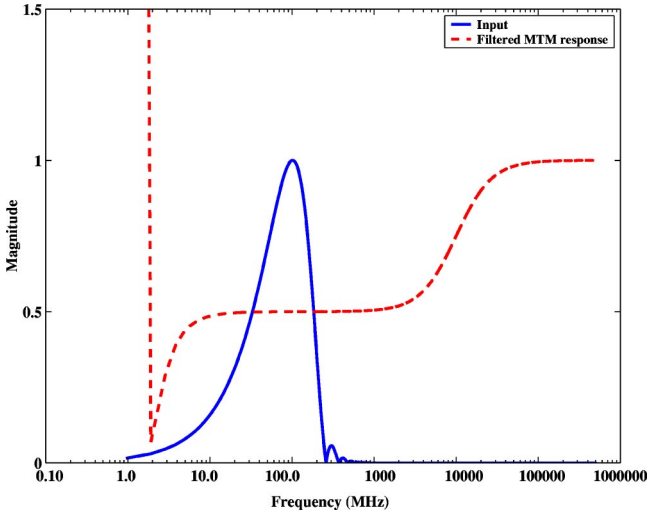

FIG. 8. (Color online) The magnitude of the spectrum of the 10.0 ns input pulse and of the magnitude of the unnormalized spectrum of the unfiltered 2TDLM MTM show very minor overlap. The effect of the low-pass filter that returns the index of refraction to 1.0 at high frequencies is clearly shown.

This is due to the approximations $\cos\beta\ell \cong 1-[(\beta l)^2/2] \cong 1$ and $\sin\beta\ell \cong \beta\ell$.

It is also well known that a transmission line can be represented by distributed lumped elements [76]. A classical per-unit-length resistance-inductance-capacitance-conductance (RLCG) representation of a segment of length Δz of lossless transmission line is shown in Fig. 10. We will call this segment a unit cell of the lumped element transmission line. The effective capacitance and inductance of the impedance and admittance elements for unit cell are simply $L_{eff}=L\Delta z$ and $C_{eff}=C\Delta z$, respectively, where L and C are, respectively, the per-unit-length values of the inductance and capacitance. Voltages V_1 and V_2 are related as $V_2=V_1-j\omega L\Delta z I_1$; currents I_1 and I_2 are related as $I_1=I_2+j\omega C\Delta z V_2$. These equations can be written in the matrix form as

$$\begin{pmatrix} 1 & -j\omega L\Delta z \\ 0 & 1 \end{pmatrix}\begin{pmatrix} V_1 \\ I_1 \end{pmatrix} = \begin{pmatrix} 1 & 0 \\ j\omega C\Delta z & 1 \end{pmatrix}\begin{pmatrix} V_2 \\ I_2 \end{pmatrix}. \tag{31}$$

This matrix equation is readily solved to give

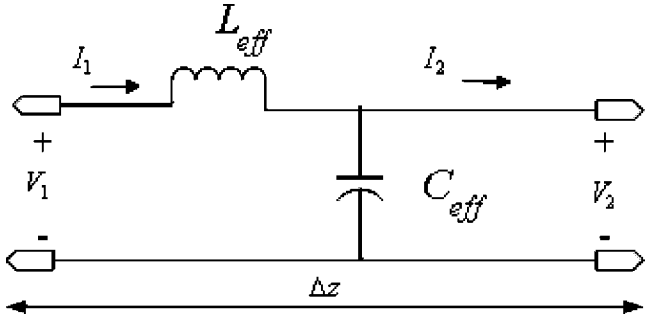

FIG. 10. Circuit model representation of a free-space transmission line.

$$\begin{pmatrix} V_1 \\ I_1 \end{pmatrix} = \begin{pmatrix} 1-\omega^2 L_{eff} C_{eff} & j\omega L_{eff} \\ j\omega C_{eff} & 1 \end{pmatrix} \begin{pmatrix} V_2 \\ I_2 \end{pmatrix}, \tag{32}$$

from which the equivalent $ABCD$ matrix is then readily extracted:

$$\begin{pmatrix} A & B \\ C & D \end{pmatrix} = \begin{pmatrix} 1-\omega^2 L_{eff} C_{eff} & j\omega L_{eff} \\ j\omega C_{eff} & 1 \end{pmatrix}. \tag{33}$$

If it is assumed that the medium associated with the lossless transmission line is free space, then L and C are equal to the free-space permeability and permittivity, respectively, i.e., $L=\mu_0$ and $C=\varepsilon_0$. Thus, the characteristic impedance and the propagation constant of the corresponding lumped element model are equal to the free-space wave values:

$$\eta = \sqrt{\frac{j\omega L_{eff}}{j\omega C_{eff}}} = \sqrt{\frac{L}{C}} = \sqrt{\frac{\mu_0}{\varepsilon_0}} \equiv \eta_0,$$

$$\beta = \omega\sqrt{LC} = \omega\sqrt{\varepsilon_0\mu_0} \equiv \beta_0. \tag{34}$$

Consequently, propagation along this lumped element transmission line model mimics propagation in free space. Other media could be represented by other ε and μ assignments. Note that if $\Delta z/\lambda \ll 1$, then the term $1-\omega^2 L_{eff} C_{eff} = 1-(\omega/c)^2(\Delta z)^2 = 1-4\pi^2(\Delta z/\lambda)^2 \approx 1$ and the $ABCD$ matrix Eq. (33) for the free-space, lumped element transmission line model becomes

$$\begin{pmatrix} A & B \\ C & D \end{pmatrix}_{FS-TL} = \begin{pmatrix} 1 & j\omega\mu_0\Delta z \\ j\omega\varepsilon_0\Delta z & 1 \end{pmatrix}. \tag{35}$$

Cascading many of these unit cells together would produce a free-space transmission line of any specified length. Approximate equivalence between the exact and the resulting cascaded lumped element total $ABCD$ matrix rests solely on the closeness of the approximation of Eq. (33) by the unit cell result Eq. (35), and this clearly depends on the electromagnetic size of the unit cell.

While this argument reveals a fundamental theoretical limitation of the lumped element model, it also reveals a practical advantage. For practical design and fabrication purposes, the unit cell size must be selected large enough for ease of construction. We know that the exact solution is recovered when $\Delta z \to 0$. Thus, if a reasonable sized lumped parameter transmission line model of a TVS medium is developed and if its wave propagation characteristics mimic those of the exact medium, there is a high probability that a realistic experimental verification of those properties can occur. Such an approach is typical and very effective in the design of microwave circuits; it is the one used below. Thus, if we can determine a lumped parameter model of the 2TDLM medium and if it predicts the TVS behavior, then basically an experiment could be fielded to demonstrate the TVS effects.

To this end, we note that the $ABCD$ matrix corresponding to Fig. 10 can also be derived in terms of the effective impedance Z_{eff} and admittance Y_{eff} as a product of the $ABCD$ matrices for the independent impedance segment and the admittance segment:

$$\begin{pmatrix} A & B \\ C & D \end{pmatrix} = \begin{pmatrix} 1 & Z_{eff} \\ 0 & 1 \end{pmatrix} \times \begin{pmatrix} 1 & 0 \\ Y_{eff} & 1 \end{pmatrix} = \begin{pmatrix} 1+Z_{eff}Y_{eff} & Z_{eff} \\ Y_{eff} & 1 \end{pmatrix}. \tag{36}$$

With $Z_{eff}=j\omega L_{eff}$ and $Y_{eff}=j\omega C_{eff}$ this result clearly recovers Eq. (33).

A TVS 2TDLM MTM lumped element transmission line is constructed immediately as follows. Using the 2TDLM frequency-domain susceptibility given in Eq. (14), one can introduce the following effective impedance and admittance elements:

$$Z_{eff} = j\omega\mu_0[1+\chi(\omega)]\Delta z, \tag{37}$$

$$Y_{eff} = j\omega\varepsilon_0[1+\chi(\omega)]\Delta z. \tag{38}$$

Therefore, the $ABCD$ matrix is given by Eq. (36) with these parameters and the impedance and wave number of the TVS 2TDLM transmission line unit cell become

$$\eta(\omega) = \sqrt{\frac{\mu(\omega)}{\varepsilon(\omega)}} = \sqrt{\frac{\mu_0}{\varepsilon_0}} = \eta_0, \tag{39}$$

$$k = \omega\sqrt{\varepsilon(\omega)\mu(\omega)} = \omega\sqrt{\varepsilon_0\mu_0}[1+\chi(\omega)], \tag{40}$$

where χ is given by Eq. (14) with the TVS values $\chi_\alpha = 1.0$, $\chi_\beta = 1.0\times10^{-5}$, $\chi_\gamma = -0.5$, $\omega_p = \omega_0 = 2\pi f_0$ and $\Gamma = 1.0\times10^{-3}\omega_0$, where $f_0 = 1.0\times10^6$ Hz.

To uncover the analytical behavior of the TVS 2TDLM transmission line (TL) unit cell, a MATLAB code was developed, which was used to implement Eqs. (36)–(38). The impedance equation (37) and admittance equation (38) of the TVS 2TDLM TL can be decomposed, respectively, into an effective capacitance C_{eff} and its effective conductance or equivalent resistance RY_{eff}, and an effective inductance L_{eff} and its effective resistance R_{eff}. These are the lumped element quantities associated with the 2TDLM TL unit cell. Their behavior as a function of frequency are shown in Figs. 11(a) and 11(b). The relative values $L_r = L_{eff}/\mu_0$ and $C_r = C_{eff}/\varepsilon_0$ are plotted in Fig. 11(a). Because their relative values have been designed to be the same, these curves are identical. The resistance values are plotted in Fig. 11(b). We note from Figs. 11(a,b) that L_{eff} and C_{eff} switch from positive to negative values at the 1.0 MHz resonance frequency of the TVS 2TDLM MTM and then switch back to positive values at 2.0 MHz. We note in Fig. 11(b) that the resistances are always positive, hence, the unit cell is strictly passive.

Since the 2TDLM MTM is lossy and dispersive near the resonance and has unusual properties at higher frequencies, it is useful to further understand the propagation characteristics for the proposed TVS 2TDLM TL unit cell. With $jk(\omega) = \alpha(\omega) + j\beta(\omega)$, its $\omega-\beta$ dispersion diagram is given in Fig. 12 for the frequencies near the resonance. Furthermore, to understand better the speeds associated with the TVS 2TDLM TL unit cell, Fig. 13 compares the phase and group

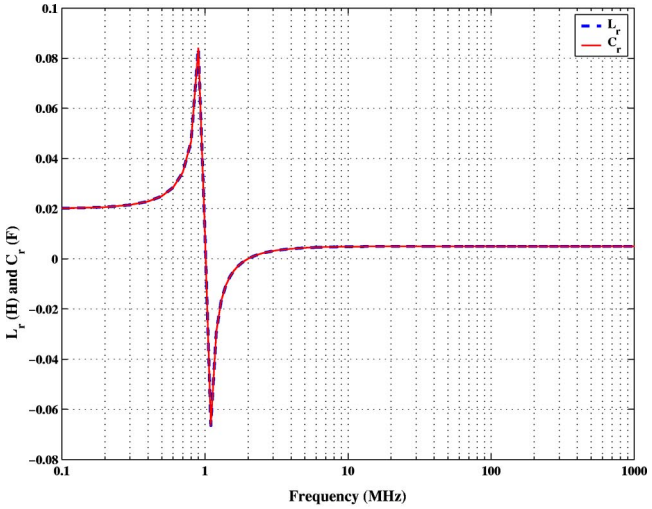

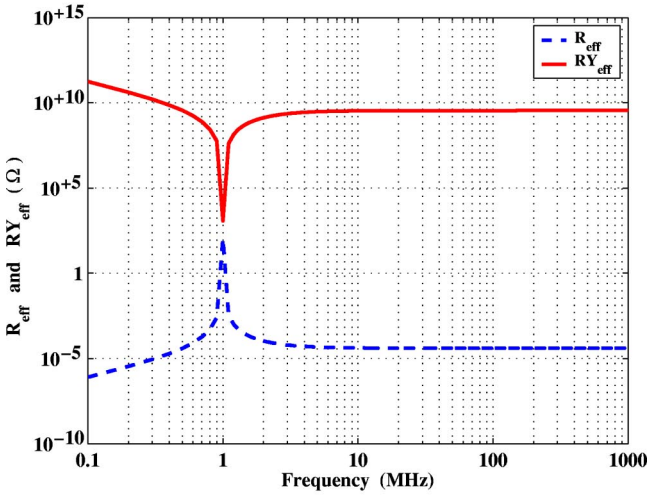

FIG. 11. (Color online) The behavior of (a) the effective inductance and capacitance and (b) associated effective resistances that define the 2TDLM TL unit cell are shown as functions of the frequency.

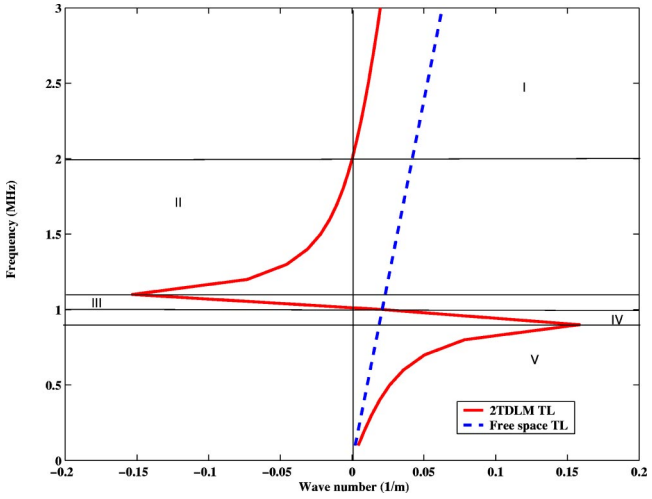

FIG. 12. (Color online) The ω-β diagram of the TVS 2TDLM TL unit cell explains many of its dispersion properties.

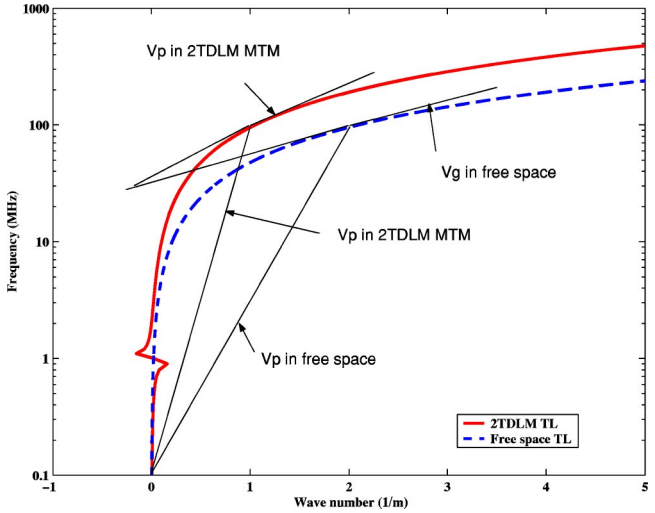

FIG. 13. (Color online) The phase and group speeds of the TVS 2TDLM TL unit cell are compared to those of free space. The TVS behavior is very apparent.

speeds of free space with those for the unit cell. These speeds are obtained from their definitions and from the dispersion relations (Fig. 12):

$$v_p^{freespace} = \frac{\omega}{\beta} = \frac{1}{\sqrt{\mu_0 \varepsilon_0}} = c, \tag{41}$$

$$v_p^{2TDLM} = \frac{\omega}{\beta} = \frac{c}{\{1 + \mathrm{Re}[\chi(\omega)]\}}. \tag{42}$$

Similarly, the group speed in both mediums can be obtained from

$$v_g^{freespace} = v_p^{freespace} = c, \tag{43}$$

$$v_g^{2TDLM} = \frac{1}{d\beta/d\omega} = \frac{c}{1 + \mathrm{Re}[\chi] + \omega \partial_\omega \{\mathrm{Re}[\chi]\}}. \tag{44}$$

The curves in Fig. 13 show that both the phase and group speeds along the 2TDLM TL are significantly greater than those in free space at 100 MHz. Therefore, if a pulse has a majority of its spectrum centered near 100 MHz, it will propagate along the TVS 2TDLM TL unit cell with speeds in excess of its speed in vacuum, as it did in the plane wave case.

To correlate both Figs. 12 and 13, the dispersion diagram in Fig. 12 is divided into several frequency bands and the phase and group speed characteristics in these bands are summarized in Table I. Clearly, in regions I and V, both the phase and group speeds are positive. However, in regions II and IV, the phase speed and the group speed have opposite signs. In region III, the phase velocity, group velocity, ε, μ, and the index of refraction are all negative. These behaviors recover many of the LH (high-pass) transmission line (''backward wave'') characteristics reported in Refs. [59–

TABLE I. The propagation characteristics of the 2TDLM MTM transmission line near the 2TDLM resonance.

Region	Phase velocity	Group velocity	ϵ and μ	Refractive index
I	>0	>0	$\epsilon>0,\ \mu>0$	$n>0$
II	<0	>0	$\epsilon<0,\ \mu<0$	$n<0$
III	<0	<0	$\epsilon<0,\ \mu<0$	$n<0$
IV	>0	<0	$\epsilon>0,\ \mu>0$	$n>0$
V	>0	>0	$\epsilon>0,\ \mu>0$	$n>0$

62. Note that these figures imply that one could tailor the operating points of a 2TDLM MTM TL for a variety of applications.

This unit cell was also modeled with Hewlett-Packard's advanced design system (HP-ADS) software tools. The HP-ADS software is commercially available and has been validated extensively against experiment. One of the main data outputs from HP-ADS is the effective scattering parameters of the circuit. The relationships between these *S* parameters and the elements of the *ABCD* matrix for any two-port network are given by the following expressions [75]:

$$\begin{pmatrix} S_{11} & S_{12} \\ S_{21} & S_{22} \end{pmatrix} = \begin{pmatrix} \dfrac{A+B/Z_0-CZ_0-D}{A+B/Z_0+CZ_0+D} & \dfrac{2(AD-BC)}{A+B/Z_0+CZ_0+D} \\ \dfrac{2}{A+B/Z_0+CZ_0+D} & \dfrac{-A+B/Z_0-CZ_0+D}{A+B/Z_0+CZ_0+D} \end{pmatrix}. \tag{45}$$

A comparison of the MATLAB predicted S_{21} results for the TVS 2TDLM TL and the free space TL unit cells of length $\Delta z=0.01$ m are shown in Fig. 14. In Fig. 14(a) the magnitude of S_{21} is shown; the phase is shown in Fig. 14(b). As one can see, the TVS 2TDLM TL is relatively lossy near the resonance, 1.0 MHz; but it is extremely low loss away from there, as expected. The percent difference in these magnitude values for the free space and the 2TDLM TL unit cells is less than 0.0001% from 2 MHz to 200 MHz. Thus, there is very little difference between the magnitudes of S_{21} for the 2TDLM TL and the free space TL unit cells in the region of interest.

Note that the magnitude of S_{21} for the 2TDLM TL at the resonance frequency 1.0 MHz is -2.69 dB. This represents the major difference in magnitude between the 2TDLM TL and the free space TL unit cells; it is due to the loss near the resonance associated with the TVS 2TDLM MTM. It was expected that this loss near the 1.0 MHz resonance frequency would become increasingly greater as the number of unit cells that are cascaded together increases. Similarly, the extremely low loss near 100 MHz would be maintained and possibly even lowered. These magnitude variations and the corresponding phase variations are shown, respectively, in Figs. 15(a) and 15(b) for 2TDLM TLs consisting of 1, 30, and 300 unit cells. As shown, there is insignificant change in the magnitude of S_{21} away from the 2TDLM MTM resonance. On the other hand, we find that the phase variations are large near the resonance and, as expected, become oscillatory as the wavelength decreases for the fixed length of the unit cell. Note that there is zero phase shift right at the resonance since the 2TDLM MTM matches free space there. With these results, one would expect no amplitude decay for a pulse that propagates along the TVS 2TDLM TL. One may, however, have some concerns that the observed phase variations at different frequencies may have a negative impact on the overall pulse propagation along it. Note, however, that one should not expect that the free space and TVS 2TDLM TLs will have the same phase properties, since the propagation characteristics in these two cases will remain different. Moreover, the change in phase with frequency should be larger for the faster speed TVS 2TDLM TL, as in Fig. 14(b). The MATLAB generated results in Figs. 14 and 15 acted as a baseline comparison case for the HP-ADS results.

To represent the TVS 2TDLM TL in HP-ADS, a two-port element had to be created, which had the same frequency characteristics. This was achieved by normalizing the MATLAB calculated impedance and the *S*-parameter values to the characteristic wave impedance of free space, 376.7Ω, according to the following relations:

$$\mathcal{Z}=\sqrt{\mathcal{Z}_0}(\mathcal{I}-\mathcal{S})^{-1}(\mathcal{I}+\mathcal{S})\sqrt{\mathcal{Z}_0}, \tag{46}$$

$$\mathcal{S}_\Omega=\sqrt{\mathcal{Y}_\Omega}(\mathcal{Z}-\mathcal{Z}_\Omega)(\mathcal{Z}+\mathcal{Z}_\Omega)^{-1}\sqrt{\mathcal{Z}_\Omega}, \tag{47}$$

where S is an $n\times n$ generalized S matrix, I is an $n\times n$ identity matrix, $\mathcal{Z}_0$ is a diagonal matrix having the characteristic impedance of each port, $\mathcal{Z}$ is the element's unique impedance matrix, and $\mathcal{Z}_\Omega$ and $\mathcal{Y}_\Omega$ are both diagonal matrices having the desired impedance and admittance as their values respectively. One then uses the normalized raw MATLAB data to generate a TOUCHSTONE formatted data file that represents the desired element. The Touchstone data file is an ASCII text file in which the properties of the element appear line by line for each frequency value. The HP-ADS software reads the TOUCHSTONE data file and treats it as a user defined device. Consequently, this acts like a lookup table of values for the TVS 2TDLM properties. Excellent agreement ($<0.001\%$ difference in magnitude and phase) between the MATLAB and the HP-ADS results for the TVS 2TDLM TL two-port element were obtained.

The simulated, long-length transmission line was designed in HP-ADS as a cascaded set of these basic elements. Two different configurations were considered, each consisting of two basic elements. These configurations are both represented in HP-ADS by the schematic diagram shown in Fig. 16. These two basic elements are labeled *A* and *B*; their combination was assumed to have the total length $\Delta z=0.02$ m. In the first case, termed the TVS-only unit cell, elements *A* and *B* were identical TVS 2TDLM TL elements, each having length $\Delta z=0.01$ m. In the second case, termed the TL-TVS unit cell, element *A* was one free-space TL element and element *B* was one TVS 2TDLM TL element, each

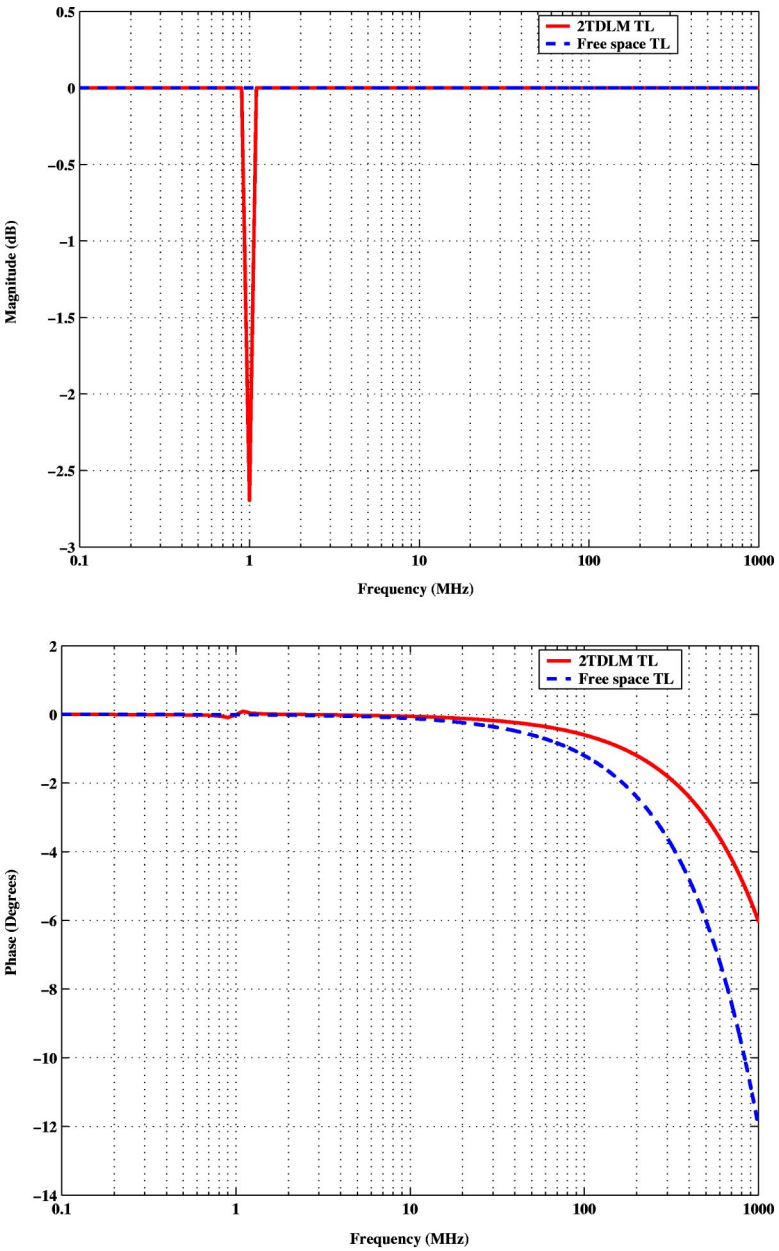

FIG. 14. (Color online) The 2TDLM and free space TL unit cells show very similar characteristics except near the resonance of the 2TDLM MTM at 1.0 MHz. (a) Magnitude of S_{21}. (b) Phase of S_{21}.

having length $\Delta z = 0.01$ m. Since the cost of fabricating each TVS 2TDLM TL element may be high, the TL-TVS unit cell design halves the total difficulty (and possibly cost) of its construction. Additionally, this type of unit cell was used successfully in Refs. [59–62] to model the LH TL configuration studied there. However, this design does impact the realized speed of any pulse propagating along it, since half the elements produce free-space speeds. These two configurations were considered as the unit cells for the cascaded TL designs. A free-space TL unit cell was also used for comparison purposes; it was obtained with both elements A and B being free-space TL elements of length $\Delta z = 0.01$ m.

The HP-ADS results for the TVS-only unit cell agreed with the MATLAB generated results for two cascaded elements as well as for a single element with twice the length with errors that were less than 0.001% in both magnitude and phase. Similarly, the MATLAB results for the TL-TVS unit cell were generated using the cascaded $ABCD$ matrices:

$$\begin{pmatrix} A & B \\ C & D \end{pmatrix} = \begin{pmatrix} \cos(\beta_0 \Delta z) & jZ_0 \sin(\beta_0 \Delta z) \\ jY_0 \sin(\beta_0 \Delta z) & \cos(\beta_0 \Delta z) \end{pmatrix} \times \begin{pmatrix} 1 + Z_{eff} Y_{eff} & Z_{eff} \\ Y_{eff} & 1 \end{pmatrix}, \tag{48}$$

where the effective impedance $Z_{eff} = j\omega\mu_0[1+\chi(\omega)]\Delta z$ and the effective admittance $Y_{eff} = j\omega\varepsilon_0[1+\chi(\omega)]\Delta z$ are those associated with the unit cell of the TVS 2TDLM TL. Excellent agreement ($<0.005\%$ difference in both magnitude and phase) between the MATLAB and the HP-ADS results for the TL-TVS unit cell were also obtained. A summary of the HP-ADS predicted S parameters for the TVS-

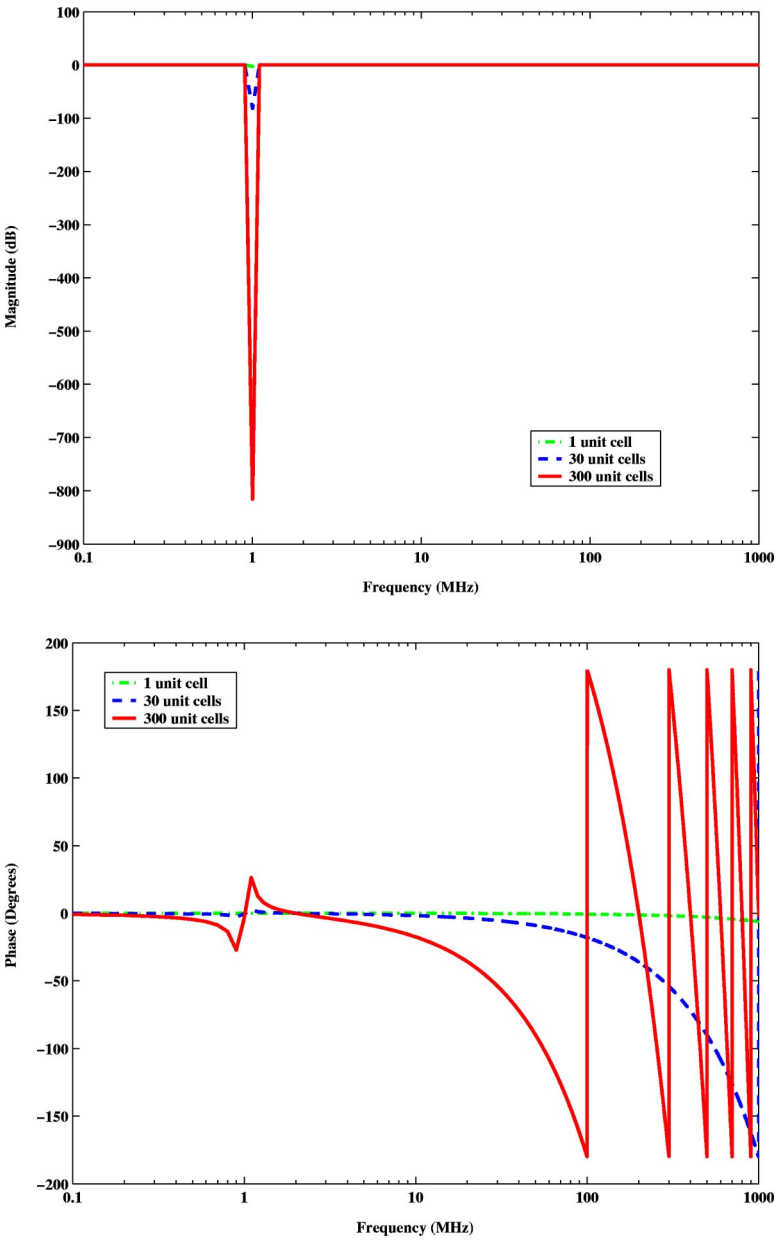

FIG. 15. (Color online) The operating characteristics of a 2TDLM TL consisting of 1, 30, and 300 unit cells are compared. (a) Magnitude of S_{21}. (b) Phase of S_{21}.

only, the TL-TVS, and the free-space unit cell transmission lines is summarized in Table II for 1.0 MHz and 100.0 MHz.

To study the behavior of a pulse as it propagates along a TVS 2TDLM TL, a TL of sufficient length had to be realized. We choose to model a transmission line having a total length of 6.0 m. This extended length of TL was achieved by cascading 300 of the TL unit cells together. Both the TVS-only and the TL-TVS unit cell TL's were considered along with the corresponding free-space TL. The HP-ADS predicted values for the magnitude and phase of S_{21} and for the impedance of the TVS-only 2TDLM TL are shown in Fig. 17. A summary of the HP-ADS predicted S parameters for the TVS-only, the TL-TVS, and the free-space 6.0 m transmission lines is given in Table III for 1.0 MHz and 100.0 MHz. Excellent magnitude, phase, and impedance behaviors were obtained in each case near 100.0 MHz. Thus, we felt that any of these designs would produce reliable results in the time domain as well.

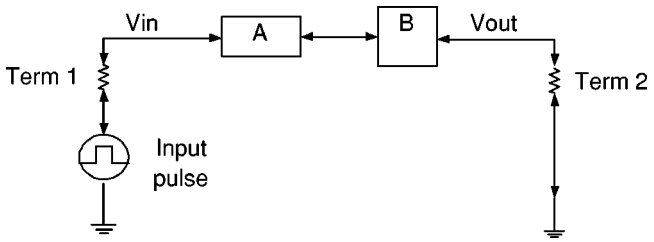

FIG. 16. Schematic diagram of the basic cascaded two-element TL models used in the HP-ADS simulations.

Because of the available pulse shapes in HP-ADS, we used a 10 ns single cycle unit amplitude pulse with a 10.0 ns bipolar width and 0.5 ns rise and fall times, which is defined explicitly as

TABLE II. Selected HP-ADS predicted, frequency domain S_{21} values for the 0.02 m long unit sections of the 2TDLM MTM transmission lines.

TL class	Frequency (MHz)	S_{21} magnitude (dB)	S_{21} phase (degrees)	Impedance (ohms)
TVS-TVS	1	-5.401	-0.024	421.044
	100	-1.914×10^{-6}	-1.202	376.917
TL-TVS	1	-2.695	-0.024	405.084
	100	-9.429×10^{-7}	-1.801	376.958
TL-TL	1	1.929×10^{-15}	-0.024	377
	100	0	-2.402	377

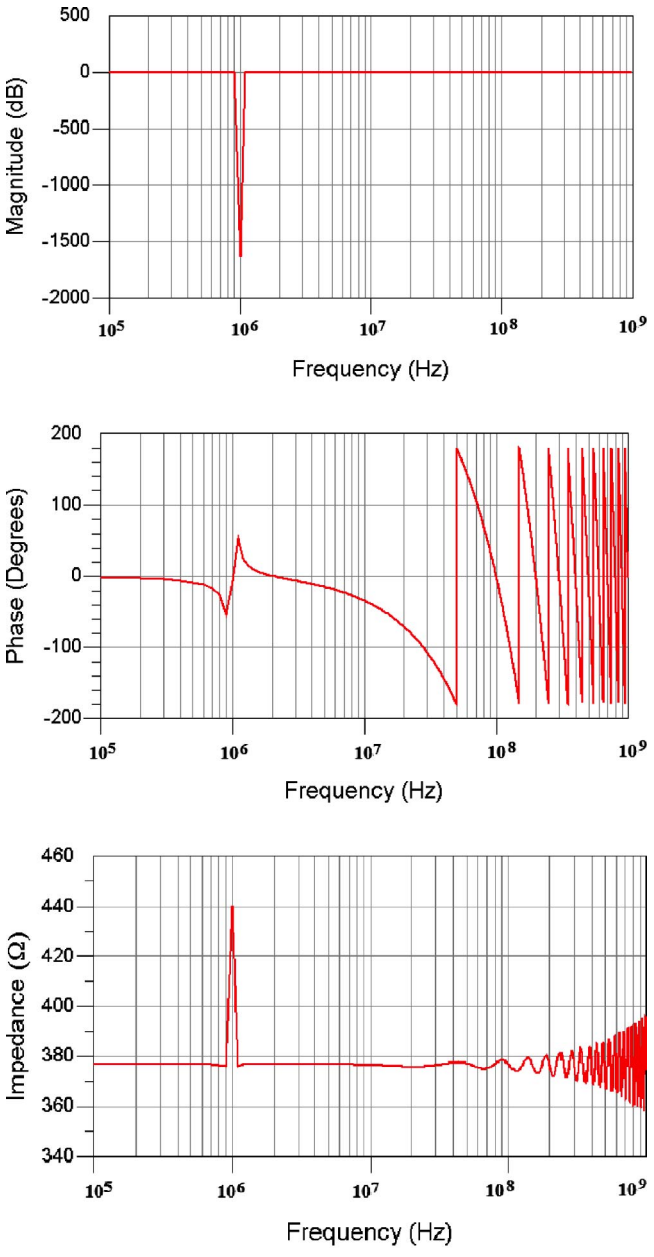

FIG. 17. The values of the S_{21} magnitude (a) and phase (b), and the TL impedance (c) for the cascaded TVS 2TDLM TL were obtained with the HP-ADS simulator.

$$f(t)=\begin{cases} 0 \quad \text{for } t<0 \text{ ns} \\ t/t_0 \quad \text{for } 0 \text{ ns} \leqslant t<0.5 \text{ ns} \\ 1 \quad \text{for } 0.5 \text{ ns} \leqslant t<4.5 \text{ ns} \\ 1-(t-t_1)/t_0 \quad \text{for } t_1=4.5 \text{ ns} \leqslant t<5.5 \text{ ns} \\ -1 \quad \text{for } 5.5 \text{ ns} \leqslant t<9.5 \text{ ns} \\ -1+(t-t_2)/t_0 \quad \text{for } t_2=9.5 \text{ ns} \leqslant t<10.0 \text{ ns} \\ 0 \quad \text{for } t>10.0 \geqslant \text{ ns}, \end{cases} \tag{49}$$

where $t_0=0.5$ ns. The center frequency of this trapezoidal pulse is located at 77.8 MHz, slightly below the 100 MHz peak of the smooth bipolar pulse equation (24).

In the HP-ADS pulse simulation runs, the pulse equation (49) was input to the TVS-only cascaded TL, the TL-TVS cascaded TL, and the free-space cascaded TL. The transient convolution analysis in HP-ADS was set to sweep from 0.0 s to 30.0 ns with 0.1 ps time steps. Unfortunately, the causality checks in HP-ADS's convolution algorithm prevented it from completing in the TVS cases. We then resorted to using the HP-ADS generated S_{21} values in a MATLAB code that was created to mimic the convolution approach. The input pulse was sampled with 3 333 334 points at the rate $\Delta t=3.0\times10^{-12}$ s from $t=0$ to $t=10.0$ μs. The HP-ADS S-parameter data consisted of 10 001 values equally spaced, from 0 Hz to 1 GHz. This data was zero padded out to 333.334 GHz. The input spectrum and the S_{21} data were multiplied together and the combination was inverse fast Fourier transformed back to the time domain.

The input pulse and the output pulses for the TVS-only cascaded TL, for the TL-TVS cascaded TL, and for the free-space cascaded TL are shown simultaneously in Fig. 18. In comparison to the input pulse shape, the distortions one observes in Fig. 18 in all of the propagated output pulse wave forms result mainly from the truncation of the S_{21} data. Negligible pulse energy is dissipated near the resonance. Analogous results are obtained using the corresponding MATLAB generated S_{21} data. More frequency data points mitigate the distortions; but the frequency truncation, such as one would expect in an experimental situation, adds more realism to the simulated data.

The magnitudes of the pulse spectra of the input pulse and the TVS-only output pulse are shown in Fig. 19. Very close agreement between the input and output pulse spectra is

TABLE III. Selected HP-ADS predicted, frequency domain S_{21} values for the 6.0 m long cascaded 2TDLM MTM transmission lines.

TL class	Frequency (MHz)	S_{21} magnitude (dB)	S_{21} phase (degrees)	Impedance (ohms)
TVS-only	1	-1631.616	-7.197	440.268
	100	-1.0×10^{-3}	-0.139	376.965
TL-TVS	1	-815.782	-7.157	440.268
	100	-2.786×10^{-4}	179.683	376.993
Free space TL	1	-7.715×10^{-15}	-7.205	377
	100	1.927×10^{-15}	-0.429	377

maintained except near the 2TDLM resonance at 1.0 MHz and after the S_{21} truncation frequency at 1.0 GHz.

Finally, to understand the sensitivity of the design, different values of the unit length and of the loss parameter Γ in the TVS 2TDLM MTM were studied. The total length of the transmission line in all the cases was maintained at 6.0 m. The results are summarized in Table IV. We found that the percentage errors in the magnitude and phase of S_{21} began to increase rapidly if the unit cell exceeded 10.0 cm. However, the results were still reasonable even for the 10.0 cm unit cell case. The smaller length cells produced even better transmission characteristics.

VII. PROPOSED TVS 2TDLM TL EXPERIMENT

Because finding RF components that would have the designed frequency dependence associated with the TVS 2TDLM TL may be extremely difficult, it was decided to design a TL with lumped elements whose capacitance, inductance, and resistance were frequency independent and which would still recover the TVS effects. We believe that this design will have the best chance of being realized experimentally.

From the above discussions, we know that the values of Z_{eff} and Y_{eff} in the TVS 2TDLM TL are frequency dependent. The first frequency-independent unit cell TL configuration is shown in Fig. 20. It contained two identical combinations of frequency-independent RLC elements; each combination reproduced the S_{21} results of the TVS-only 2TDLM TL at 100 MHz. A second frequency-independent unit cell TL configuration was obtained by replacing the first TVS-only RLC-TL element in Fig. 20 with a frequency independent free-space RLC-TL element. This second unit cell reproduced the S_{21} results of the TL-TVS 2TDLM TL at 100 MHz. In both the cases, each unit element had the same length, $\Delta z=0.01$ m and hence, the unit cells were each $\Delta z=0.02$ m long. The values of the frequency-independent lumped elements in both the cases were extracted from the exact values of the corresponding frequency-dependent elements at 100 MHz: $R_{eff}=4.0284\times10^{-5}\ \Omega$, $L_{eff}=6.28137\times10^{-9}$ H$=6.281$ nH, $G_{eff}=1/RY_{eff}=1/(2.838\,29\times10^{-10}\ \Omega)=3.523\,25\times10^{+9}$ mho$=3.523$ Gmho, and $C_{eff}=4.425\,62\times10^{-14}$ F$=44.26$ fF.

The magnitude of S_{21}, the phase of S_{21}, and the impedance predicted by HP-ADS for the 300 unit element cascaded TVS-only RLC-TL are given in Figs. 21(a, b, and c).

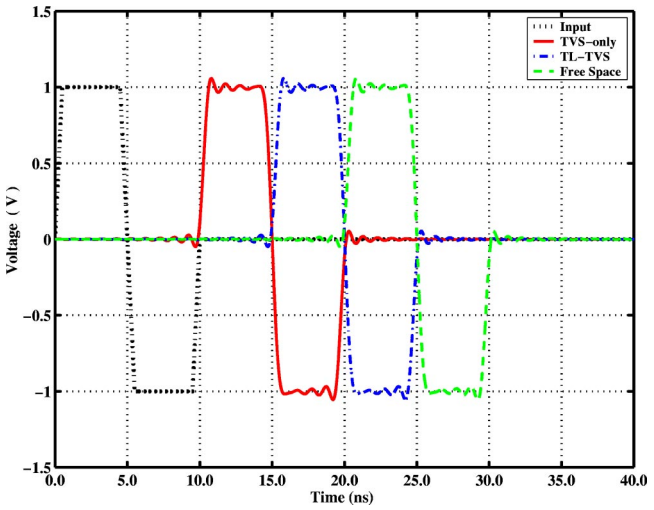

FIG. 18. (Color online) The pulses received at $z=6$ m after propagation through the free-space TL (dashed-dot green line), the TVS-only TL (solid red line), and the TL-TVS TL (blue dashed line) are compared. The TVS effects are readily apparent. Very minor distortion of the input pulse is present in the propagated results.

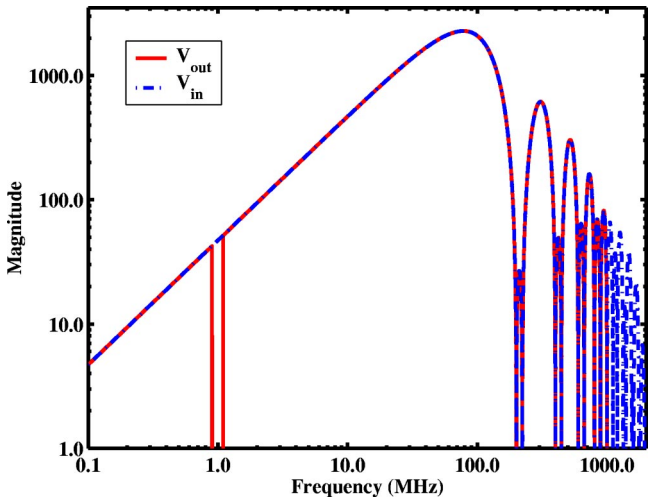

FIG. 19. (Color online) The spectra of the $z=6$ m TVS-only transmission line output pulse and the input pulse show only small variations between them.

TABLE IV. Summary of the HP-ADS S_{21} simulation results for different unit cell lengths and 2TDLM loss parameter Γ for a fixed total length 6.0 m TVS-only TL at 100 MHz.

2TDLM	$\Delta z = 1.0$ m		$\Delta z = 10.0$ cm		$\Delta z = 1.0$ cm		$\Delta z = 1.0$ mm	
Γ	dB	Degrees	dB	Degrees	dB	Degrees	dB	Degrees
1.0×10^{-1}	-7.9011	167.16	-2.743×10^{-2}	179.44	-2.732×10^{-2}	179.68	-2.732×10^{-2}	179.69
1.0×10^{-3}	-7.8824	167.03	-2.799×10^{-4}	179.44	-2.786×10^{-4}	179.68	-2.786×10^{-4}	179.69
1.0×10^{-5}	-7.8822	167.03	-8.358×10^{-6}	179.44	-8.194×10^{-6}	179.68	-8.193×10^{-6}	179.69

The S parameters were swept from 0 Hz to 30.0018 GHz with 100 kHz steps. Table V contains explicit values for each of the RLC-TL cases at the 2TDLM resonance frequency 1.0 MHz and at the center frequency 100.0 MHz of the smooth bipolar pulse. Excellent agreement (errors for both the magnitude and phase were $<0.001\%$) between these results and the corresponding frequency-dependent ones was obtained at 100 MHz. Large errors were realized at the resonance frequency 1.0 MHz, but this was expected since the large frequency variations of the 2TDLM MTM occur only near the resonance. Thus, either the lumped element TVS-only RLC-TL or the corresponding TL-TVS RLC-TL would be quite satisfactory for propagation experiments for pulses whose spectra are centered near 100 MHz.

The pulse propagation experiments for the TVS-only RLC-TL and the TL-TVS RLC-TL were run completely with the time domain solver in HP-ADS. This was now possible because the elements were frequency independent and the explicit time integration package in HP-ADS was applicable. The input and output pulses measured at 6.0 m are compared to those obtained from the free-space TL, in Fig. 22. The TVS effect is clearly maintained even with these frequency-independent based RLC-TLs. The corresponding magnitudes of the spectra of the input and output wave forms for the frequency-independent TVS-only and the TL-TVS TLs show little distortion during the propagation of the input pulse along those TLs. Note that it was found that the HP-ADS predicted peaks of the spectra appear to occur nearer to 100 MHz, slightly higher than the more exact 77.8 MHz value obtained with the MATLAB code. This was a direct result of the fewer number of points used in the HP-ADS calculation to achieve a timely conclusion of the calculations.

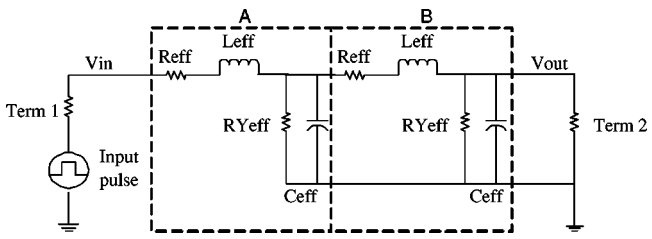

FIG. 20. Schematic diagram of the frequency-independent TVS-only RLC-TL unit cell used in the HP-ADS simulations.

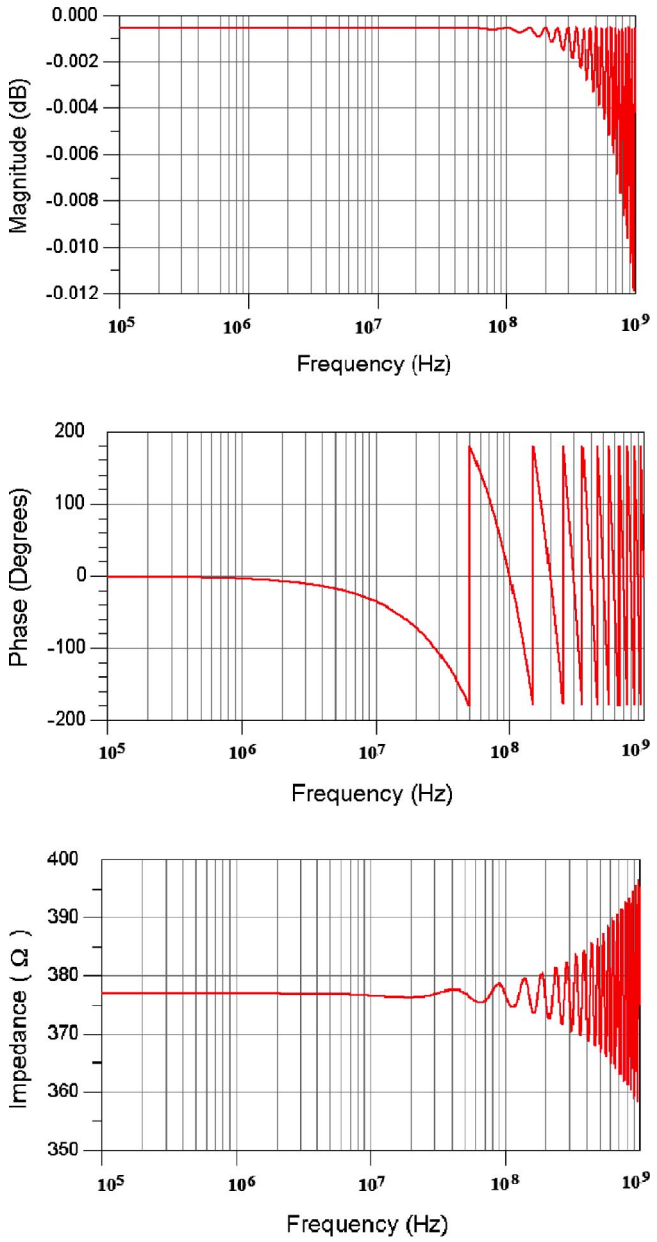

FIG. 21. The frequency-independent TVS-only RLC-TL results agree extremely well with the frequency-dependent TVS-only TL results away from the 2TDLM resonance at 1.0 MHz. (a) Magnitude of S_{21}. (b) Phase of S_{21}. (c) TL impedance.

TABLE V. Selected HP-ADS predicted, frequency domain S_{21} values for the frequency-independent, 6.0 m long 2TDLM MTM transmission lines.

TL class	Frequency (MHz)	S_{21} magnitude (dB)	S_{21} phase (degrees)	Impedance (ohms)
TVS-only	1	-0.001	-1.0×10^{-3}	376.995
	100	-0.001	-1.0×10^{-3}	376.941
TL-TVS	1	-2.786×10^{-4}	-5.403	405.084
	100	-2.786×10^{-4}	179.683	376.958
Free space TL	1	-7.715×10^{-15}	-7.205	377
	100	1.927×10^{-15}	-0.429	377

To check these calculations further, the pulse propagation along the TL-TVS RLC-TL was also modeled with SPICE, a well-known circuit simulator. Similar results were obtained.

From Fig. 22 we found that the HP-ADS predicted output pulse front arrives at the observation point 20.03 ns after the input pulse has been initiated on the free-space transmission line. It arrives 10.05 ns after the input pulse has been initiated on the TVS-only RLC-TL. It arrives 14.83 ns after the input pulse has been initiated on the TL-TVS RLC-TL. The expected theoretical delays and the simulated delays are summarized in Table VI. The measured front speeds were $1.991c$, $1.539c$ (average speed), and $0.999c$, respectively, for the TVS-only, TL-TVS, and the free-space RLC-TLs. These results clearly indicate that the pulse travels at trans-vacuum speeds through the passive, frequency-independent lumped element, 2TDLM MTM based transmission lines without violating causality. Moreover, because these TLs are lossy and dispersive and because the numerics imposes its own loss and dispersion characteristics, the fact that the spectral properties of the input pulses were basically maintained during the entire propagation length suggests that these TVS 2TDLM RLC-TLs will be robust in their practical implementation. We have identified commercially available components that could be used to carry out this experiment; preliminary simulations of the experiment have reproduced the predicted TVS results.

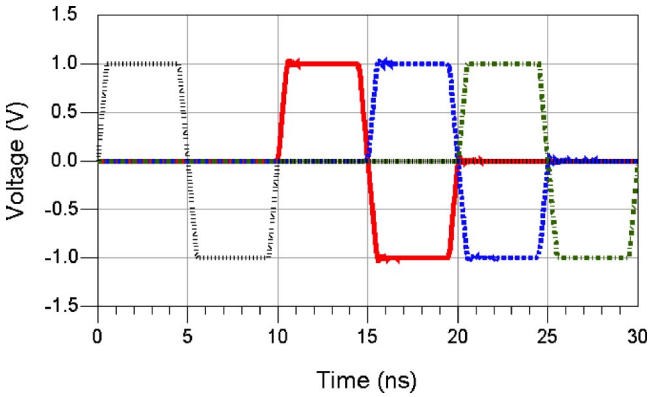

FIG. 22. (Color online) The 10.0 ns input pulse ($z=0$ m, dotted black line) and the pulses received at $z=6$ m after propagation through the frequency independent TVS-only (solid red line) and TL-TVS TL (dashed blue line) are compared to the free-space TL result (dot-dashed green line). Very minor distortion of the input pulse is present in the propagated results. The TVS effect is clearly seen.

VIII. CONCLUSIONS

The existence of passive trans-vacuum-speed metamaterials, in which the speed of light is greater than its speed in vacuum has been demonstrated. The TVS metamaterial was designed using a two-time-derivative Lorentz material model. Analytical and numerical results for the propagation of plane waves in a 2TDLM TVS medium were used to validate these TVS properties. A transmission line realization of the dispersive 2TDLM TVS medium was established. Excellent agreement between the results of the theoretical plane wave constructs and the corresponding transmission line models was demonstrated. A practical, frequency-independent transmission line TVS MTM design was extracted and validated numerically. It suggests that the TVS TL results could be confirmed experimentally. Such an experiment based on this TVS MTM TL design is now in the final design stages.

ACKNOWLEDGMENTS

This work was supported in part by INTEL Corp. Several of the calculations performed were enabled by the generous donation by INTEL Corp. of a DELL 530 workstation. The authors would like to thank INTEL Corp. for their support. R.W.Z. would also like to thank George Eleftheriades for several very interesting conversations concerning the equivalent circuit models for wave propagation in DNG media and for sharing his recent results during the Quantum Optics Workshop at the Kavli Institute for Theoretical Physics in July 2002. This interaction was supported in part by the National Science Foundation under Grant No. PHY99-07949.

TABLE VI. Pulse propagation characteristics along the 6.0 m long, frequency-independent 2TDLM MTM transmission lines.

Design case	Time delay (ns)	Speed (m/s)
TVS	10.05	$1.991c$
TL-TVS	14.83	$1.539c$ (average)
Free space TL	20.03	$0.999c$

[1] C.G.B. Garrett and D.E. McCumber, Phys. Rev. A **1**, 305 (1970).
[2] J. Peatross, S.A. Glasgow, and M. Ware, Phys. Rev. Lett. **84**, 2370 (2000).
[3] R. Donnelly and R.W. Ziolkowski, Proc. R. Soc. London, Ser. A **440**, 541 (1993).
[4] J.-Y. Lu and J.F. Greenleaf, IEEE Trans. Ultrason. Ferroelectr. Freq. Control **39**, 19 (1992).
[5] R.W. Ziolkowski, A.M. Shaarawi, and I.M. Besieris, J. Opt. Soc. Am. B **10**, 75 (1993).
[6] J.-Y. Lu and J.F. Greenleaf, IEEE Trans. Ultrason. Ferroelectr. Freq. Control **39**, 441 (1992).
[7] H. Friedrich, Am. J. Phys. **63**, 183 (1995).
[8] M. Mojahedi, E. Schamiloglu, F. Hegeler, and K.J. Malloy, Phys. Rev. E **62**, 5758 (2000).
[9] X.-J. Zhou, Phys. Lett. A **278**, 1 (2000).
[10] D. Mugnai, A. Ranfagni, and R. Ruggeri, Phys. Rev. Lett. **84**, 4830 (2000).
[11] A.P.L. Barbero, H.E. Hernandez-Figueroa, and E. Recami, Phys. Rev. E **62**, 8628 (2000).
[12] G. Nimtz and A. Haibel, Ann. Phys. (Leipzig) **11**, 163 (2002).
[13] M. Xiao, Opt. Lett. **25**, 995 (2000).
[14] R.Y. Chiao, Phys. Rev. A **48**, R34 (1993).
[15] E.L. Bolda, R.Y. Chiao, and John C. Garrison, Phys. Rev. A **48**, 3890 (1993).
[16] A.M. Steinberg and R.Y. Chiao, Phys. Rev. A **49**, 2071 (1994).
[17] E.L. Bolda, J.C. Garrison, and R.Y. Chiao, Phys. Rev. A **49**, 2938 (1994).
[18] R.Y. Chiao, Quantum Opt. **6**, 359 (1994).
[19] R.Y. Chiao and J. Boyce, Phys. Rev. Lett. **73**, 3383 (1994).
[20] R.Y. Chiao, J. Boyce, and M.W. Mitchell, Appl. Phys. B: Lasers Opt. **B60**, 259 (1995).
[21] A.M. Steinberg and R.Y. Chiao, Phys. Rev. A **51**, 3525 (1995).
[22] R.Y. Chiao, E. Bolda, J. Bower, J. Boyce, J.C. Garrison, and M.W. Mitchell, Quantum Semiclassic. Opt. **7**, 279 (1995).
[23] L.J. Wang, A. Kuzmich, and A. Dogariu, Nature (London) **406**, 277 (2000).
[24] A. Kuzmich, A. Dogariu, L.J. Wang, P.W. Milonni, and R.Y. Chiao, Phys. Rev. Lett. **86**, 3925 (2001).
[25] P.W. Milonni, J. Phys. B **35**, R31 (2002).
[26] Quantum Optics Workshop, The Kavli Institute for Theoretical Physics, 2002. See http:\\www.kavli.ucsb.edu
[27] R.W. Ziolkowski, Phys. Rev. E **63**, 046604 (2001).
[28] R.W. Ziolkowski, IEEE Trans. Antennas Propag. **45**, 656 (1997).
[29] R.W. Ziolkowski, Phys. Rev. E **55**, 7696 (1997).
[30] R.W. Ziolkowski and F. Auzanneau, J. Appl. Phys. **82**, 3195 (1997).
[31] R.W. Ziolkowski and F. Auzanneau, J. Appl. Phys. **82**, 3192 (1997).
[32] F. Auzanneau and R.W. Ziolkowski, J. Phys. III **7**, 2405 (1997).
[33] F. Auzanneau and R.W. Ziolkowski, J. Electromagn. Waves Appl. **12**, 353 (1998).
[34] F. Auzanneau and R.W. Ziolkowski, IEEE Trans. Microwave Theory Tech. **46**, 1628 (1998).
[35] F. Auzanneau and R.W. Ziolkowski, IEEE Trans. Antennas Propag. **47**, 1330 (1999).
[36] R.W. Ziolkowski, Phys. Rev. E **55**, 7696 (1997).
[37] R.W. Ziolkowski, IEEE Trans. Antennas Propag. **45**, 1530 (1997).
[38] R.W. Ziolkowski, Comput. Methods Appl. Mech. Eng. **169**, 237 (1999).
[39] D.C. Wittwer and R.W. Ziolkowski, IEEE Trans. Antennas Propag. **48**, 192 (2000).
[40] D.C. Wittwer and R.W. Ziolkowski, IEEE Trans. Antennas Propag. **48**, 200 (2000).
[41] D.C. Wittwer and R.W. Ziolkowski, IEEE Trans. Microwave Theory Tech. **49**, 250 (2001).
[42] V.G. Veselago, Sov. Phys. Usp. **10**, 509 (1968).
[43] D.R. Smith, W.J. Padilla, D.C. Vier, S.C. Nemat-Nasser, and S. Schultz, Phys. Rev. Lett. **84**, 4184 (2000).
[44] J.B. Pendry, Phys. Rev. Lett. **85**, 3966 (2000).
[45] D.R. Smith and N. Kroll, Phys. Rev. Lett. **85**, 2933 (2000).
[46] R.A. Shelby, D.R. Smith, S.C. Nemat-Nasser, and S. Schultz, Appl. Phys. Lett. **78**, 489 (2001).
[47] R.A. Shelby, D.R. Smith, and S. Schultz, Science **292**, 77 (2001).
[48] R.W. Ziolkowski and E. Heyman, Phys. Rev. E **64**, 056625 (2001).
[49] I.V. Lindell, S.A. Tretyakov, K.I. Nikoskinen, and S. Ilvonen, Microwave Opt. Technol. Lett. **31**, 129 (2001).
[50] M.W. Feise, P.J. Bevelacqua, and J.B. Schneider, Phys. Rev. B **66**, 035113 (2002).
[51] S.A. Tretyakov, Microwave Opt. Technol. Lett. **31**, 163 (2001).
[52] C. Caloz, C.-C. Chang, and T. Itoh, J. Appl. Phys. **90**, 5483 (2001).
[53] J.A. Kong, B.-I. Wu, and Y. Zhang, Microwave Opt. Technol. Lett. **33**, 136 (2002).
[54] R. Marques, F. Medina, and R. Rafii-El-Idrissi, Phys. Rev. B **65**, 144440 (2002).
[55] A. Alu and N. Engheta, *IEEE-Nano 2002 Digest* (IEEE Press, Piscataway, NJ, 2002), p. 233.
[56] N. Fang and X. Zhang, *IEEE-Nano 2002 Digest* (IEEE Press, Piscataway, NJ, 2002), p. 225.
[57] D. Wu, N. Fang, C. Sun, X. Zhang, W. Padilla, D. Basov, and D. Smith, *IEEE-Nano 2002 Digest* (IEEE Press, Piscataway, NJ, 2002), p. 229.
[58] R.W. Ziolkowski, *IEEE-Nano 2002 Digest* (IEEE Press, Piscataway, NJ, 2002), p. 223.
[59] A.K. Iyer and G.V. Eleftheriades, *IEEE MTT-S International Microwave Symposium Digest* (IEEE, Seattle, WA, 2002), p. 1067.
[60] G.V. Eleftheriades, A.K. Iyer, and P.C. Kremer, IEEE Trans. Microwave Theory Tech. **50**, 2702 (2002).
[61] A. Grbic and G.V. Eleftheriades, IEEE Int. Symposium an Antennas and Propagation Digest, San Antonio, TX, June 16–21 2002, vol. 4, p. 340.
[62] A. Grbic and G.V. Eleftheriades, J. Appl. Phys. **92**, 5930 (2002).
[63] R.W. Ziolkowski, IEEE Trans. Antennas Propag. **51**, 1516 (2003).
[64] R.W. Ziolkowski and A. Kipple, in special issue on metamaterials, IEEE Trans. Antennas Propag. (to be published).
[65] P.W. Milonni, *The Quantum Vacuum: An Introduction to Quantum Electrodynamics* (Academic Press Inc., San Diego, CA, 1994), pp. 249–251.
[66] K. Scharnhorst, Phys. Lett. B **236**, 354 (1990).

[67] G. Barton, Phys. Lett. B **237**, 559 (1990).
[68] P.W. Milonni and K. Svozil, Phys. Lett. B **248**, 437 (1990).
[69] S. Ben-Menahem, Phys. Lett. B **250**, 133 (1990).
[70] G. Barton and K. Scharnhorst, J. Phys. A **26**, 2037 (1993).
[71] J.D. Jackson, *Classical Electrodynamics*, 2nd ed. (Wiley, New York, 1975).
[72] N. Levinson and R.M. Redheffer, *Complex Variables* (Holden-Day Inc., San Francisco, 1970), p. 159.
[73] J.A. Kong, *Electromagnetic Wave Theory* (Wiley, New York, 1986), pp. 297–299.
[74] L.D. Landau and E.M. Lifshitz, *Electrodynamics of Continuous Media* (Pergamon, New York, 1960), p. 260.
[75] David M. Pozar, *Microwave Engineering*, 2nd ed. (Wiley, Toronto, 1998), pp. 56–59.
[76] S. Ramo, J.R. Whinnery, and T. Van Duzer, *Fields and Waves in Communication Electronics*, 3rd ed. (Wiley, Toronto, 1994), pp. 257–258.